U-Pb GEOCHRONOLOGY, Sr-Nd GEOCHEMISTRY, PETROGENESIS AND TECTONIC SETTING OF GANDAB VOLCANIC ROCKS, NORTHEASTERN IRAN

AZAM ENTEZARI HARSINI[1], SEYED A MAZAHERI[1], SAEED SAADAT[2] and JOSÉ F SANTOS[3]

[1]*Department of Geology, Ferdowsi University of Mashhad, Mashhad, Iran*
[2]*Department of Geology, Mashhad Branch, Islamic Azad University, Mashhad, Iran*
[3]*Department of Geosciences, Geobiotec Research Unit, University of Aveiro, 3810-193 Aveiro, Portugal*

Abstract: This paper addresses U-Pb geochronology, Sr-Nd geochemistry, petrogenesis and tectonic setting in the Gandab volcanic rocks. The Gandab volcanic rocks belong to the Sabzevar zone magmatic arc (northeastern Iran). Petrographically, all the studied volcanic rocks indicate porphyritic textures with phenocrysts of plagioclase, K-feldespar, hornblende, pyroxene, and magnetite which are embedded in a fine to medium grained groundmass. As well, amygdaloidal, and poikilitic textures are seen in some rocks. The standard chemical classifications show that the studied rocks are basaltic trachy andesite, trachy andesite, trachyte, and trachy dacite. Major elements reveal that the studied samples are metaluminous and their alumina saturation index varies from 0.71 to 1.02. The chondrite-normalized rare earth element and mantle-normalized trace element patterns show enrichment in light rare earth elements (LREE) relative to heavy rare earth elements (HREE) and in large ion lithophile elements (LILE) relative to high field strength elements (HFSE). As well they show a slightly negative Eu anomaly (Eu/Eu* = 0.72 – 0.97). The whole-rock geochemistry of the studied rocks suggests that they are related to each other by fractional crystallization. LA-MC-ICP-MS U-Pb analyses in zircon grains from two volcanic rock samples (GCH-119 and GCH-171) gave ages ranging of 5.47 ± 0.22 Ma to 2.44 ± 0.79 Ma, which corresponds to the Pliocene period. In four samples analysed for Sr and Nd isotopes $^{87}Sr/^{86}Sr$ ratios range from 0.704082 to 0.705931 and $^{\varepsilon}Nd$ values vary between +3.34 and +5. These values could be regarded to as representing mantle derived magmas. Taking into account the comparing rare earth element (REE) patterns, an origin of the parental magmas in enriched lithospheric mantle is suggested. Finally, it is concluded that Pliocene Gandab volcanic rocks are related to the post-collision environment that followed the Neo-Tethys subduction.

Keywords: U-Pb geochronology, Sr-Nd geochemistry, post-collision, Gandab volcanic rocks, Northeastern Iran.

1. INTRODUCTION

According to limited geochronology data, magmatic activity in the eastern Iran started in the late Jurassic (Esmaiely *et al.*, 2005; Tarkian *et al.*, 1983) and continued into the Quaternary, forming a variety of volcanic and volcanoclastic rocks, as well as subvolcanic stocks (Saadat and Stern, 2016). The volcanic rocks in Iran are mainly classified into three geographical categories as follows: a belt extended from Maku area to Bazman zone, the Alborz Mountains, and east territories of Iran (Pazirandeh, 1973). The volcanic rocks in Iran have aver-

Corresponding author: S. Saadat
e-mail: saeed.saadat@colorado.edu

age andesitic composite but other types of the volcanic rocks such as rhyolite, dacite, trachyte, basalt, are also seen (Pazirandeh, 1973). This paper presents a constructive set of new U-Pb geochronology data combined with Sr-Nd isotope and geochemical data for sample of volcanic rocks from the Gandab area in northeastern Iran, and an analysis of the tectonic factors involved in their petrogenesis. It is a contribution to the understanding of magmatic activity in this part of the Alpine-Himalayan collision belt. The study area is located at 220 km southwest of the Mashhad (capital of the Razavi Khorasan Province in northeast of Iran) and 80 km south of the Neyshabour (a city in the Razavi Khorasan Province). This district is positioned from 58° 42' 15" to 58° 43' 40" east longitude and 35° 47' 30" to 35° 52' 00" north latitudes, covering 48 km^2 (Fig. 2).

2. GEOLOGICAL SETTING

The Iranian plateau surrounded between the Arabian plate to the southwest, the Eurasia plate to the northeast, the Indian oceanic plate to the south, and the Helmand/Afghanistan block to the east (Saadat et al., 2010). The collision between Arabian plate and central Iran began sometime between the end of the Eocene and before the Miocene (e.g. Berberian and King, 1981; Hatzfeld and Molnar, 2010). An expanded regime between central Iran and southern margin of Eurasia was

created in Early Cretaceous period and it formed Neo-Tethys Ocean (Shafii Moghadam et al., 2014) and narrow branch of this Neo-Tethys is known as Sabzevar Ocean (Sengor, 1990; Shafii Moghadam et al., 2014). In Late Cretaceous until Tertiary, the subduction of the oceanic crust beneath East Alborz belt caused the development of a magmatic arc (Spies et al., 1983; Shafii Moghadam et al., 2014). Tertiary intrusive and volcanic rocks of Sabzevar zone have the characteristics of the calc-alkaline magmas. Furthermore, there are alkaline rocks in this zone.

As shown in Fig. 1, Gandab area is situated in the Sabzevar structural zone, and Sabzevar Torbat Jam sub-zone at north of the Daruneh fault (e.g. Ruttner and Stöcklin, 1967; Berberian and King, 1981; Alavi, 1991) located in the central part of the 1:100000 geological map of Kadkan sheet in northeast of Iran (Naderi Mighan, 2000).

3. METHOD

Petrographic Study

163 samples were collected from the study area. Standard petrographic thin sections were prepared from these samples. The samples were examined in the laboratory of the Ferdowsi University of Mashhad, using standard techniques of optical mineralogy to determine their textures, mineral contents and rock type.
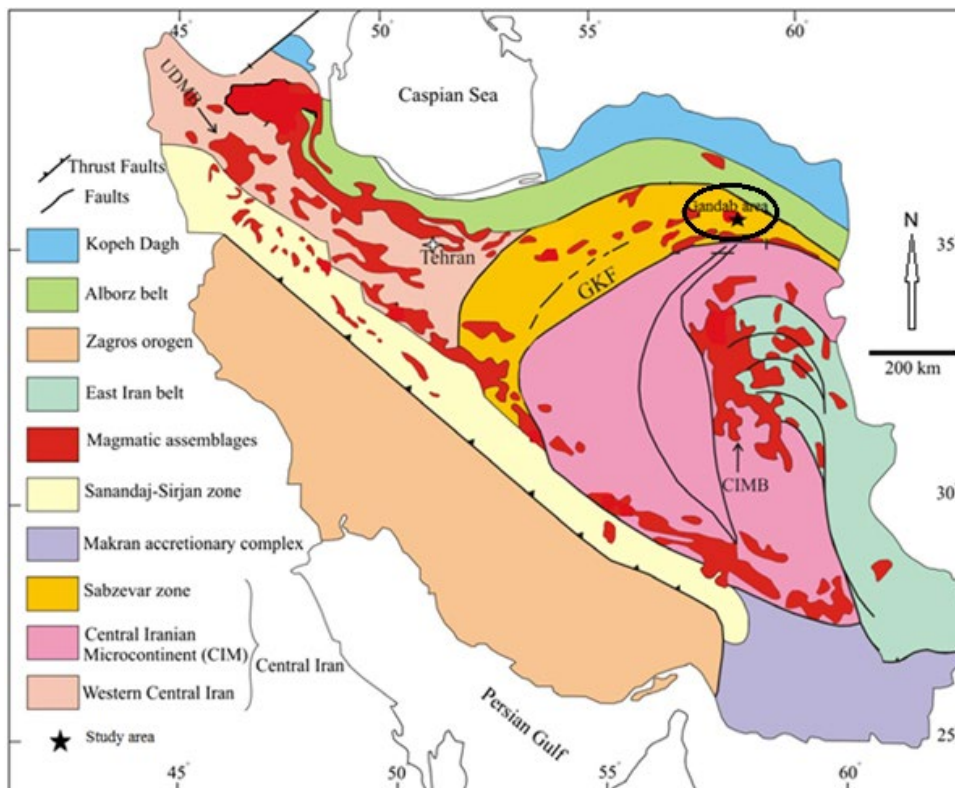

Fig. 1. *Simplified structural map of Iran (compiled from Ruttner and Stöcklin, 1967, Berberian and King, 1981, Alavi, 1991) and location of the Gandab prospecting area in the Northeast of Iran.*

Major and trace element geochemistry

After excluding weathered and altered samples, twenty Samples with no or minimum signs of alteration were selected for chemical analysis from various types of rock units. The selected samples were crushed and powdered by mild steel, and sent to kansaran Binaloud Company (Tehran, Iran) to analyze major oxides by XRF spectrometry. As well, these samples were sent to Acme laboratories (Vancouver, Canada) for trace element analysis by ICP mass spectrometry (Acme labs code 4B03 Research ICP/MS) that is carried out with lithium metaborate-tetraborate fusion and nitric acid digestion. **Table 1** indicates the geographic locations, names, and the symbols of the samples which were analyzed by XRF and ICP-MS methods.

U-Pb geochronology

According to the field study and relative age determination, two samples as the oldest (GCh-119, 6 Kg in weight) and the youngest (GCh-171, 10 Kg in weight) volcanic rocks were selected for U-Pb geochronology (**Table 3**). These samples were broken into small fragments by crusher and pulverized into fine grain and passed from 40 mesh sieve. Each sample was washed using water and acetone to get rid of clay-sized particles, and other probable undesired contaminants. After washing, samples were completely dried by suction through a vacuum line for 24-hours. The samples were then transferred into a Frantz magnetic barrier separator and each sample was divided into two non-magnetic and magnetic portions. This process was done to separate the magnetic heavy and altered ferromagnesian minerals from the samples for reducing time during the later zircon grain-picking stage. Non-magnetic heavy minerals extraction was performed by Bromoform ($CHBr_3$). Zircon grains were separated under a binocular by hand-picking. The zircon grains were sent to university of Tasmania (Australia). This analyses were performed on an Agilent 7900 quadrupole ICP-MS with a 193 nm Coherent Ar-F excimer laser and the Resonetics S155 ablation cell at the University of Tasmania in Hobart. The down hole fractionation, instrument drift and mass bias correction factors for Pb/U ratios on zircons were calculated using 2 analyses on the primary (91500 standard of Wiendenbeck *et al.*, 1995) and checked on 1 analysis on each of the secondary standard zircons (Temora standard of Black *et al.*, 2003 and JG1 of Jackson *et al.*, 2004) analysed at the beginning of the session and every 15 unknown zircons (roughly every 1/2 hour) using the same spot size and conditions as used on the samples. Additional secondary standards (The Mud Tank Zircon of Black and Gulson, 1978, Penglai zircons of Li *et al.*, 2010, and the Plesovice zircon of Slama *et al.*, 2008) were also analysed. The correction factor for the $^{207}Pb/^{206}Pb$ ratio was calculated using large spots of NIST610 analysed every 30 unknowns and corrected using the values recommended by Baker *et al.* (2004). Each analysis on the zircons began with a 30 second blank gas measurement followed by a further 30 seconds of analysis time when the laser was switched on. Zircons were sampled on 32 micron spots using the laser at 5 Hz and a density of approximately

Table 1. *Geographic location, name, and symbol of the analyzed samples in the Gandab volcanic rocks.*

Sample	Longitude (E)	Latitude (N)	Rock type	Symbol
GCh-171	58°44'25"	35°48'59"	Pyroxene andesite	⊕
GCh-92	58°44'27"	35°48'39"	Pyroxene andesite	⊕
GCh-119	58°43'39"	35°47'37"	Hornblende pyroxene olivine trachy andesite basalt	⋈
GCh-154	58°41'42"	35°50'53"	Hornblende pyroxene olivine trachy andesite basalt	⋈
GCh-131	58°42'08"	35°49'23"	Olivine hornblende trachy andesite basalt	⊠
GCh-179	58°41'24"	35°49'24"	Olivine hornblende trachy andesite basalt	⊠
GCh-60	58°42'49"	35°49'55"	Pyroxene hornblende trachy andesite	■
GCh-17	58°43'12"	35°49'49"	Pyroxene hornblende trachy andesite	■
GCh-140	58°42'34"	35°50'50"	Hornblende andesite	◆
GCh-35	58°42'58"	35°50'02"	Hornblende andesite	◆
GCh-160	58°41'38"	35°50'03"	Hornblende trachy andesite	◆
GCh-183	58°43'12"	35°49'33"	Hornblende trachy andesite	◆
GCh-16	58°43'27"	35°49'49"	Trachy andesite	▲
GCh-71	58°43'14"	35°49'31"	Trachy andesite	▲
GCh-40	58°43'09"	35°50'03"	Trachy andesite	▲
GCh-31	58°43'02"	35°50'09"	Trachy andesite	▲
GCh-57	58°42'44"	35°50'18"	Hornblende pyroxene trachy andesite	+
GCh-86	58°43'37"	35°49'14"	Hornblende pyroxene trachy andesite	+
GCh-27	58°43'16"	35°50'00"	Andesite	✳
GCH-49	58°42'53"	35°50'14"	Andesite	✳

2 J/cm^2. A flow of carrier gas at a rate of 0.35 litres/minute carried particles ablated by the laser out of the chamber to be mixed with Ar gas and carried to the plasma torch. Isotopes measured were ^{49}Ti, ^{56}Fe, ^{90}Zr, ^{178}Hf, ^{202}Hg, ^{204}Pb, ^{206}Pb, ^{207}Pb, ^{208}Pb, ^{232}Th, ^{235}U and ^{238}U with each element being measured every 0.17 s with longer counting time on the Pb isotopes compared to the other elements. The data reduction used was based on the method outlined in detail in Halpin *et al.* (2014) and is similar to that outlined in Black *et al.* (2004) and Paton *et al.* (2010). Uncertainties were calculated using methods similar to that outlined Halpin *et al.* (2014) and Paton *et al.* (2010). Element abundances on zircons were calculated using the method outlined by Kosler (2001) using Zr as the internal standard element, assuming stoichiometric proportions and using the NIST610 to standard correct for mass bias and drift.

Sr-Nd isotopic analyses

Based on the petrographic and elemental geochemical information, four samples of the volcanic rocks of Gandab area were selected and sent to the Laboratory of Isotope Geology of the Aveiro University (Portugal) for Sr and Nd isotopic analysis (**Table 4**). The selected powdered samples were dissolved by HF/HNO$_3$ solution in PTFE-lined Parr acid digestion bombs at a temperature of 180°C for 3 days. After evaporation of the final solution, the samples were dissolved in HCl (6.2 N) and also in acid digestion bombs, and dried again. The elements to analyze were purified using conventional ion chromatography technique in two stages: separation of Sr and REE in ion exchange columns containing AG8 50 W Bio-Rad cation exchange resin, followed by separation of Nd from other lanthanides in columns containing cation exchange resin Eichrom Ln resin. All reagents used in the preparation of the samples were sub-boiling distilled, and the water produced by a Milli-Q Element (Millipore) apparatus. Strontium was loaded with H$_3$PO$_4$ on a single Ta filament, whereas Nd was loaded with HCl on a Ta outer side filament in a triple filament arrangement. Both Sr and Nd isotopic ratios were determined by a multi-collector Thermal Ionization Mass Spectrometer (TIMS) VG Sector 54. Data were acquired in dynamic mode with peak measurements at 1–2 V for ^{88}Sr and 0.5–1.0 V for ^{144}Nd. Typical runs consisted of acquisition of 60 isotopic ratios. Strontium and neodymium isotopic ratios were corrected for mass fractionation relative to ^{88}Sr/^{86}Sr = 0.1194 and ^{146}Nd/^{144}Nd = 0.7219. During this study, the SRM-987 standard gave an average value of ^{87}Sr/^{86}Sr = 0.710263(17) (N = 13; confidence limit = 95 %) and the JNdi-1 standard gave an average value of ^{143}Nd/^{144}Nd = 0.5121031(66) (N = 13; confidence limit = 95%).

4. PETROGRAPHY

Andesitic rocks are dominant in the study area and middle Eocene coarse bedded limestone rocks folded and trusted above these volcanic rocks (**Fig. 2**). Based on the mineral assemblage and their percentage, andesitic volcanic rocks of the Gandab area can be classified into 9 sub-groups as follows. These groups are sorted by age from old to new respectively.

Hornblende pyroxene olivine basaltic andesite

Outcrops of these volcanic rocks are observed in the south, north, and northeast (**Fig. 2**) and display a porphyritic texture with microlitic groundmass. Plagioclase (25–30 vol. %), olivine (15–20 vol. %), clinopyroxene (10–15 vol. %), opacity hornblende (8–10 vol. %), and magnetite (5–7 vol. %) are the dominant phenocryst phases. Phenocryts occurs as large euhedral crystals, and plagioclases mostly display polysynthetic twins and some of them show slight oscillatory zoning. As well, some clinopyroxens show augite twins (**Fig. 3a**). Furthermore, Olivine grains are replaced by iddingsite and serpentine; opacity hornblendes are replaced by chlorite.

Olivine hornblende basaltic andesite

According to the field mapping (**Fig. 2**), these rocks are seen in the south and southwest. Olivine hornblende basaltic andesites have porphyritic textures with medium grained groundmass and in some parts they have current microlitic matrix. The mineralogy of this unit contains large euhedral phenocryst of plagioclase (20–25 vol. %), opacity hornblende and normal hornblende (7–10 vol. %), olivine (5–8 vol. %), magnetite (4–5 vol. %), and a small amount of clinopyroxen (0–5 vol. %). Olivine grains have been widely iddingsited (**Fig. 3b**).

Pyroxene hornblende trachy andesite

Pyroxene hornblende trachy andesite is mainly observed in the center of the area (**Fig. 2**) with porphyritic texture and fine grained groundmass. Microlitic, glomeroporphyritic and amygdaloidal textures are seen as well. Some of these rock's vesicles have been filled by carbonate and jarosite. The euhedral phenocrysts of these rocks are plagioclase (7–14 vol. %), K-feldspar (5–10 vol. %), subhedral phenocrysts of normal and opacity hornblendes (5–7 vol. %), magnetite (4–5 vol. %) (**Fig. 3c**), and clinopyroxenes (2–5 vol. %). Plagioclases, hornblendes, and groundmass are hardly carbonatic and epidotic.

Hornblende pyroxene trachy andesite

Hornblende pyroxene trachy andesites are seen in the center, northeast, and east of the Gandab area (**Fig. 2**). The dominant texture of these rocks are porphyritic with microlitic medium grained groundmass. Moreover, glomeroporphyritic and poikilitic texture (**Fig. 3d**) are seen. These rocks contain euhedral phenocrysts of plagioclase (5–10 vol. %), K-feldspar (5–8 vol. %), opacity hornblende (5–7 vol. %), and subhedral clinopyroxene (3–6 vol. %).

Hornblende andesite

Field observations show that hornblende andesites are located in the east and north of the area (**Fig. 2**). Majority of the rocks have texture of porphyritic with fine grained groundmass and in some sections microlitic as well as amygdaloidal texture with vesicles filled by carbonate, epidote and secondary iron oxide. In this lithology, phenocryst phases are dominated by euohedral plagioclase with slightly polysynthetic twins (7–15 vol. %), euhedral to subhedral opacity hornblende (3–8 vol. %), and magnetite (3–5 vol. %) (**Fig. 3e**). In some places, the secondary iron oxide veinlet is observed with 0.01 mm diameter. In addition, phenocrysts and groundmass have been moderately altered to carbonate, epidote, chlorite, and clay minerals.

Andesite

Andesits are found at the north and center of the area (**Fig. 2**). These rocks have porphyritic texture, with subhedral or euhedral phenocrysts of plagioclase (5–7

vol. %), and minor hornblende (< 2 vol. %). Furthermore, in some parts they contain amygdals of carbonate and chlorite (**Fig. 3f**). Metasomatic alteration of the andesite rocks is evident in the groundmass and phenocrysts. In most instances, these are replaced by carbonate, epidot and mineral clay.

Hornblende trachy andesite

Hornblende trachy andesite is the most plentiful rock in this area. It is seen in the west, east, center, northeast, and southeast (**Fig. 2**). This lithology is described as rocks in which plagioclase (5–10 vol. %), opacity hornblende (4–8 vol. %), magnetite (3–7 vol. %), and K-feldspar (3–5 vol. %) are the major phenocrysts phases into fine to coarse grained groundmass or microlitic. The plagioclases are euhedral, tabular and commonly polysynthetic twins, the k-feldspar crystals are slightly smaller than the plagioclases, euhedral and commonly karlsbad twins, and the opacity hornblendes and magnetite grains are subhedral to euhedral. The phenocrysts and ground-
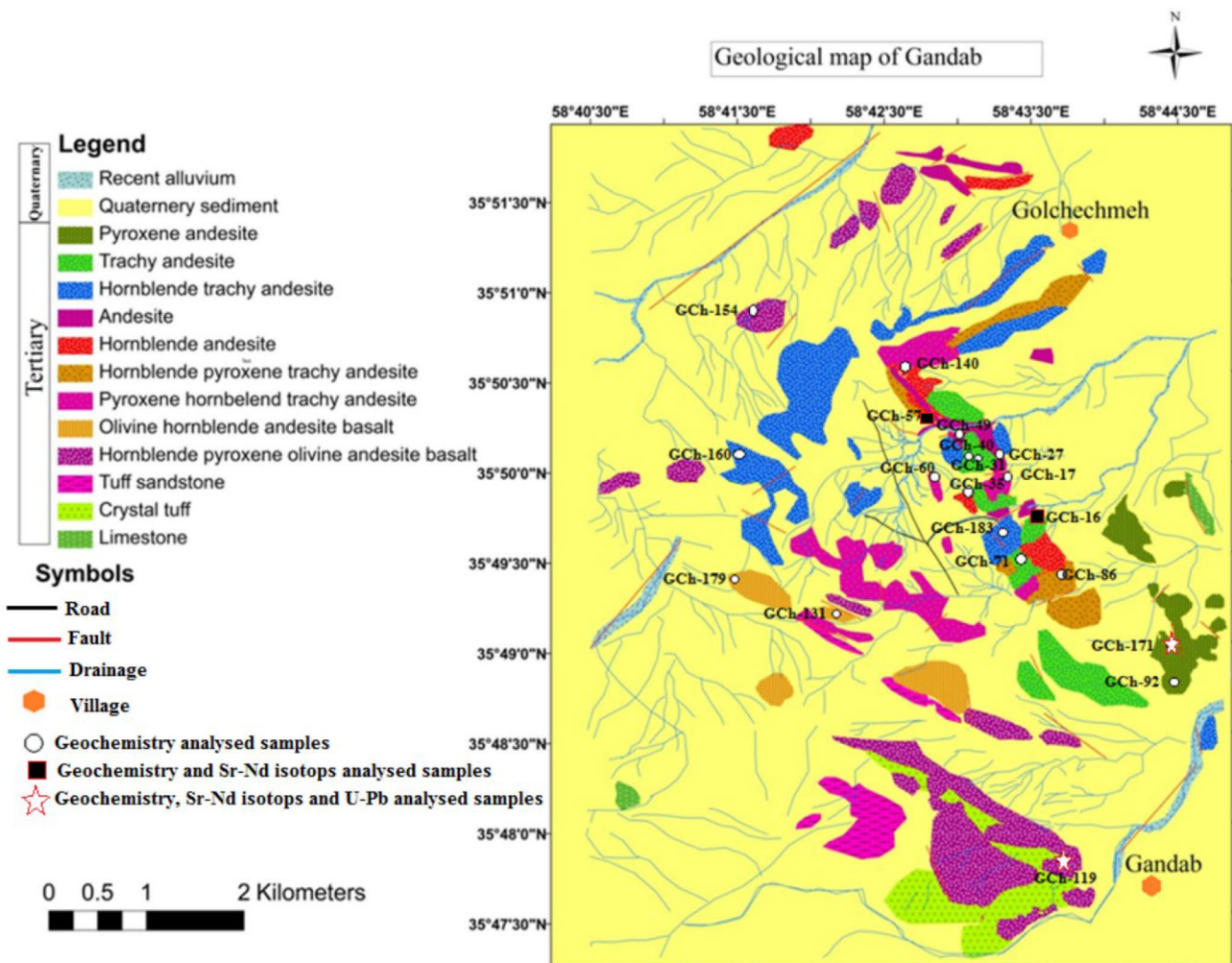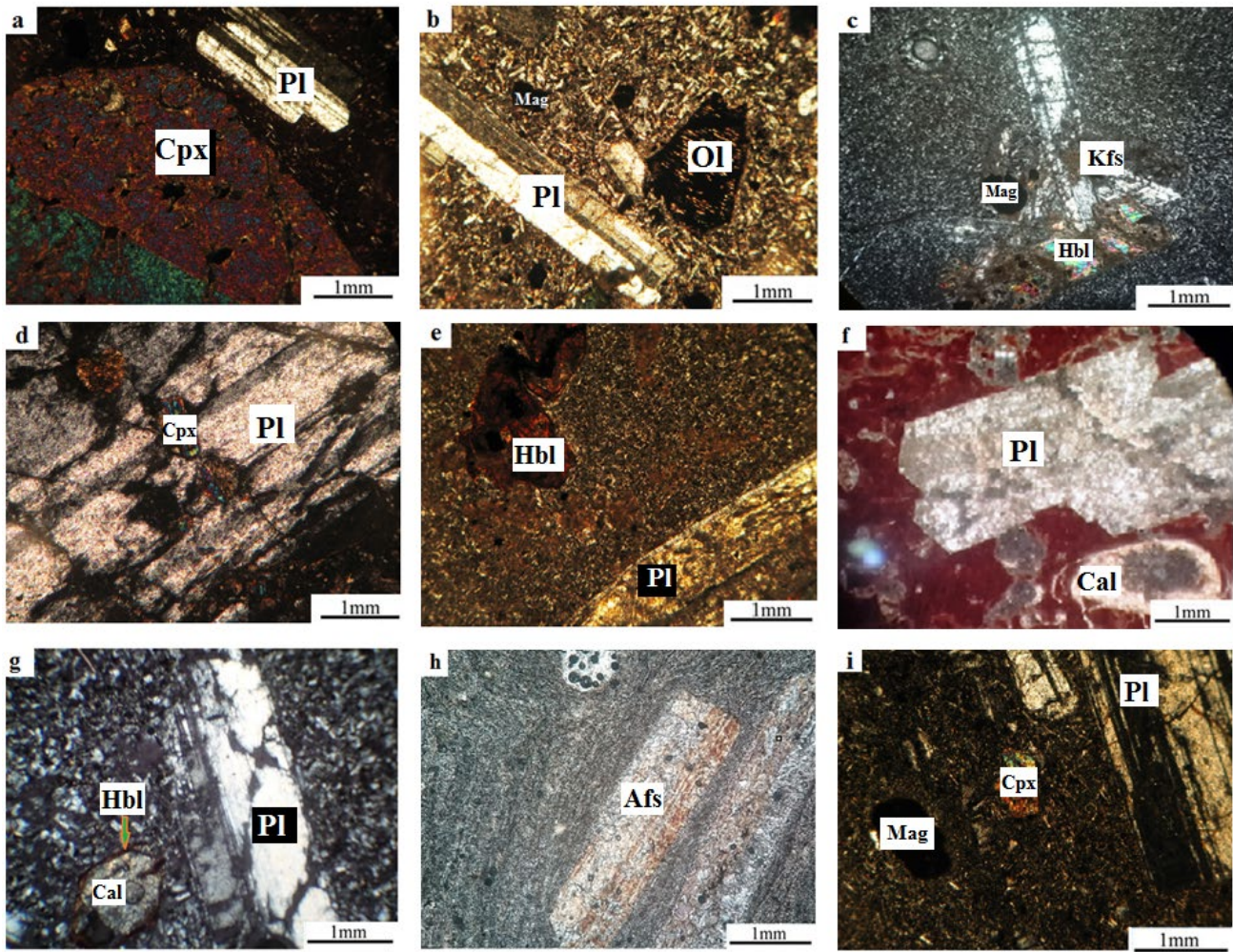

Fig. 2. *Geological map of the Gandab area (Entezari et al., 2016).*

Fig. 3. *Microscopic images of thin sections of volcanic rocks in the studied area (Entezari et al., 2016): (a) Plagioclase and pyroxene phenocrysts in microlitic groundmass in the Hornblende pyroxene olivine basaltic andesite, XPL; (b) Plagioclase and olivine phenocrysts in medium grained groundmass and converting olivine to chlorite and iddingsite in the Olivine hornblende basaltic andesite; (c) K-feldspar, hornblendel, magnetite phenocrysts, and glomeroporphyritic texture in the Pyroxene hornbelend trachy andesite; (d) Poikilitic texture in the Hornbelend pyroxene trachy andesite; (e) Plagioclase and opacity hornblende phenocrysts in the Hornblende andesite; (f) Phenocryst of plagioclase in a matrix of fine grain to intersertal and amygdals of carbonate in the Andesite; (g) Plagioclase and hornblende phenocrysts and alteration of hornblende to carbonate in the Hornblende trachy andesite; (h) K-feldspar phenocryst and trachytic texture in the Trachy andesite; (i) Plagioclase, clinopyroxene, and magnetite phenocrysts in the Pyroxene andesite.*

mass are locally and moderately altering to carbonate (**Fig. 3g**).

Trachy andesite

Trachy andesites are seen in the central and southeast parts of the area (**Fig. 2**). They have porphyritic texture with fine to medium grained groundmass as well as trachytic texture (**Fig. 3h**), and amygdaloidal filled with carbonate and chlorite are rarely seen. The main phenocrysts are euhedral plagioclase with polysynthetic twins (7–10 vol. %), K-feldspar with karlsbad twins (5–7 vol. %). Moreover, minor opacity hornblende (<1vol. %) is seen in these rocks. In some parts, these rocks show moderate alteration to carbonate and clay minerals.

Pyroxene andesite

The Pyroxene andesite is the youngest andesite volcanic rocks placed in the west Gandab area (**Fig. 2**). This lithology contains phenocrysts of euhedral plagioclase (15–30 vol. %), subherdal clinopyroxene (7–15 vol. %), and magnetite (4–5 vol. %) in a porphyritic and glomerophorphyry texture with fine to medium grains groundmass (**Fig. 3i**). Some of the vesicles have been filled by carbonate, chlorite, and secondary iron oxide. In thin sections, the carbonate, epidote, and secondary iron oxide veinlet are observed with 0.04 to 0.1 mm diameter as well as the plagioclase phenocryst and matrix is converted to the carbonate and epidote.

5. RESULTS AND DISCUSSIONS

Major and trace elements

The results of the major and trace elements for 20 samples of free to weakly altered volcanic rocks are shown in **Table 2**. The total alkali-silica (TAS) classification diagram of Middlemost (1994) is used to categorize the volcanic rocks. The volcanic collection is wholly plotted within the basaltic trachy andesite, trachy andesite, trachyte, and trachy dacite fields (**Fig. 4a**). Most samples are located in the alkaline section and boundary between alkaline and sualkaline of diagram of Irvine and Baragar (1971) (**Fig. 4b**).

All of the Gandab volcanic rocks exhibit metaluminous on the diagram of Shand (1943) (**Fig. 5**) and their geochemical character with alumina saturation index [ASI = molar Al_2O_3 / $(CaO + K_2O + Na_2O)$] is ranging from 0.71 to 1.02. By using SiO_2 as a fractionation index, MgO, FeO, and CaO contents display minus correlation with SiO_2 content, while Al_2O_3, K_2O, and Na_2O contents represent positive correlation with SiO_2 content, as well, $TiO2$ and P_2O_5 are dispersed and they show no correlation with SiO_2 content (**Fig. 6a-6h**). The linear trend among SiO_2 and several major oxides demonstrates a genetic relationship in these volcanic rocks. Na_2O, Al_2O_3, and K_2O *vs.* SiO_2 diagrams display an increasing and thin trend. This issue points out that K-feldspar and sodic plagioclases were crystallized in the late stage of crystallization and pending fractionation of a silicate melt at down pressures. Along with increasing percentage of silica, CaO, MgO, and FeO are decreased in these rocks. Probably such trends are compatible with fractionation of the seen phenocryst phases which have been created from a basaltic andesite as a parental magma. In fact, this type of variation displays that Mg and Fe-rich rock-forming minerals contain amphibole, pyroxene, and olivine and they have had a great role during the crystallization of volcanic rocks like plagioclases which represents the effect of fractional crystallization on a pending magmatic evolution. La, Nb, Zr, Rb, Th, Ta, and Hf contents are positively correlated SiO_2 concentrations (**Fig. 6i-6o**). The trace element variations in these igneous rocks are compatible with plagioclase, amphibole, and Fe-Ti oxide fractionation (Mazhari *et al.*, 2011). Multi-element spider diagrams were normalized with primitive-mantle (McDonough and Sun, 1995) (**Fig. 7a**) and indicate that the volcanic rocks are depleted in high field strength elements (HFSE) which may be owing to fractionation of a titanium-rich phase in the magma source (Ghalamghash *et al.*, 2009). Additionally, all samples present enrichment in the components of large ion lithophile elements (LILE) compared to field strength elements (HFSE) in normalized primitive-mantle diagram (**Fig. 7a**). The above mentioned characteristics point out that the volcanic rocks would belong to the subduction zones. **Fig. 7b** shows a range of chondrite-normalized distribution REE patterns (Boynton, 1984) for 20 analyzed samples of Gandab volcanic rocks. The La_N/Sm_N ratios vary between 2.35 to
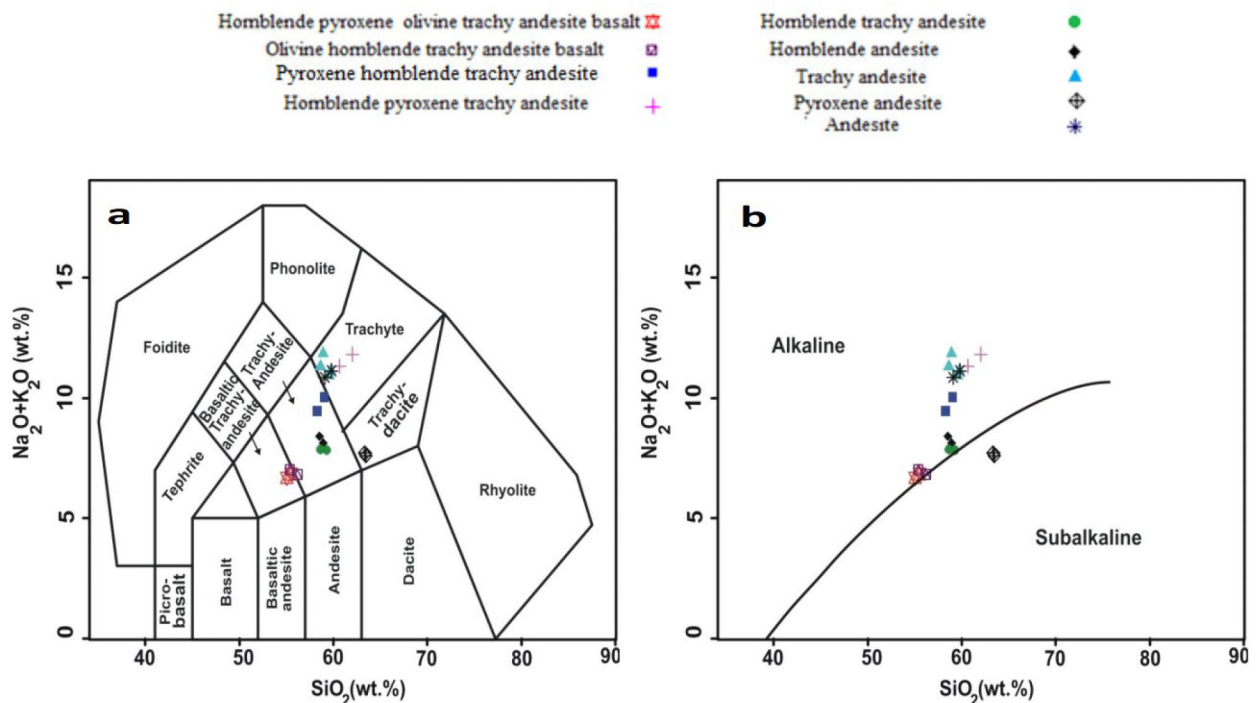
Fig. 4. *(a) Na_2O + K_2O vs. SiO_2 diagram (Middlemost, 1994); (b) diagram for discriminate between subalkaline and alkaline fields (Irvine and Baragar,1971).*

Table 2. *Major element (in wt% by XRF) and trace element (in ppm by ICP-MS) compositions of samples from Gandab volcanic rocks (Entezari et al., 2016).*

Sample	GCH-171	GCH-92	GCH-119	GCH-153	GCH-131	GCH-179	GCH-60	GCH-17	GCH-140	GCH-35	GCH-160	GCH-183	GCH-16	GCH-71	GCH-57	GCH-86	GCH-40	GCH-31	GCH-27	GCH-49
SiO_2	62.58	61.54	54.01	54.39	55.01	54.56	57.86	57.12	57.71	57.35	58.01	57.25	57.86	57.42	60.88	59.35	58.36	58.12	55.87	55.12
Al_2O_3	17.69	17.59	15.91	16.05	15.86	15.62	17.99	18.03	18.24	18.35	18.02	18.42	17.08	16.89	17.52	18.13	17.63	17.51	15.24	15.35
FeO	3.50	3.82	8.21	7.92	7.53	7.79	4.80	5.35	5.19	5.12	5.23	5.17	5.21	5.34	3.73	4.22	4.85	5.01	4.26	4.78
CaO	5.27	5.92	6.87	6.52	7.02	7.32	4.26	4.62	5.17	5.21	5.24	5.27	2.86	3.42	1.68	1.89	3.01	2.97	4.98	5.02
Na_2O	4.48	4.53	3.56	3.45	3.29	3.35	4.34	4.12	3.94	4.25	3.59	3.75	4.75	4.35	4.26	4.12	3.87	3.67	2.98	2.87
K_2O	3.02	2.95	2.99	3.25	3.38	3.57	5.49	5.15	4.02	3.98	4.08	3.92	6.89	6.72	7.34	6.95	7.02	6.99	7.41	7.25
MgO	0.27	0.42	5.24	5.10	4.52	4.98	1.78	1.98	2.35	2.37	2.34	2.52	1.69	1.91	1.48	1.79	1.49	1.78	0.98	1.35
TiO_2	1.429	1.354	0.891	0.854	0.840	0.915	0.968	1.071	0.869	0.864	0.867	0.862	1.011	1.009	0.914	1.050	0.918	0.899	1.154	1.034
MnO	0.080	0.069	0.112	0.131	0.098	0.082	0.069	0.059	0.045	0.048	0.042	0.046	0.124	0.105	0.040	0.051	0.078	0.087	0.063	0.087
P_2O_5	0.336	0.392	0.341	0.313	0.362	0.333	0.454	0.521	0.418	0.455	0.418	0.428	0.732	0.792	0.323	0.355	0.513	0.532	0.468	0.423
L.O.I	1.04	1.15	1.62	1.78	1.87	1.55	1.73	1.76	1.66	1.67	1.85	1.87	1.43	1.66	1.51	1.72	2.03	2.10	4.40	4.65
Total	99.72	99.86	99.82	99.83	99.80	99.71	99.77	99.81	99.64	99.52	99.71	99.53	99.71	99.72	99.74	99.71	99.87	99.76	99.51	99.76
Cu	0.02	0.02	0.01	0.01	0.01	0.01	0.02	0.02	0.01	0.01	0.01	0.01	0.05	0.07	0.05	0.06	0.10	0.06	1.69	1.81
S	0.009	0.008	0.054	0.057	0.009	0.008	0.012	0.013	0.012	0.015	0.008	0.009	0.018	0.035	0.011	0.019	0.008	0.009	0.017	0.017
Ba	287	294	383	367	376	381	515	552	482	475	451	453	551	525	485	435	570	552	497	505
Be	2	2	1	2	1	1	2	2	1	2	2	2	1	1	2	1	2	2	4	3
Co	4.3	5.6	27.4	28.2	28.7	29.1	9.8	10.1	12.1	12.8	12.7	13.1	8.0	9.1	4.8	5.2	7.4	6.9	6.1	5.8
Cs	1.1	1.5	1.9	2.4	2.2	2.6	2.9	3.1	1.9	1.5	1.3	1.2	3.3	2.8	3.6	3.2	3.3	2.9	3.0	2.8
Ga	19.6	18.3	16.1	15.9	15.6	16.2	15.1	15.6	18.2	18.8	17.2	16.8	15.5	16.1	16.0	15.5	15.0	14.3	13.7	14.1
Hf	7.5	7.4	2.9	2.8	2.9	2.9	3.7	3.6	3.3	3.5	3.5	3.4	3.6	3.7	4.1	4.2	3.7	3.8	3.4	3.3
Nb	27.9	26.2	9.9	10.4	11.5	10.8	15.2	15.8	14.5	14.1	14.3	14.6	16.5	16.2	19.2	18.8	15.8	15.6	15.3	15.7
Rb	68.0	73.1	70.8	72.4	74.4	79.1	135.4	142.1	97.0	110.2	96.1	82.2	160.4	155.2	182.2	173.1	158.7	148.9	144.9	145.5
Sn	3	2	2	1	1	2	2	2	1	2	1	1		1	1	1	1	1	1	
Sr	453.9	438.2	614.8	580.3	559.8	592.2	608.6	595.1	726.7	717.3	728.7	731.2	504.7	491.2	239.1	251.2	454.3	432.1	347.2	371.1
Ta	1.8	1.6	0.6	0.7	0.7	0.8	0.9	0.8	0.8	0.9	1.0	0.8	1.1	1.0	1.2	1.1	0.9	1.0	1.0	0.9
Th	9.1	9.5	3.7	4.3	4.1	4.8	6.1	6.2	4.9	5.1	5.0	4.8	7.2	6.9	7.8	7.4	6.7	7.1	6.2	6.3
U	2.7	2.5	1.1	1.3	1.1	1.2	1.6	1.4	1.4	1.6	1.5	1.4	2.3	2.5	1.1	1.1	2.3	2.4	2.4	2.1
V	112	120	259	262	252	243	298	310	265	256	269	285	395	375	223	259	361	345	279	242
W	1.4	1.6	1.5	1.9	2.9	3.1	1.3	1.7	1.5	1.8	1.7	1.5	1.4	1.6	2.0	1.8	1.8	1.6	3.3	2.7
Zr	306.1	297.3	108.6	121.5	119.8	109.1	157.9	149.1	142.0	138.5	140.9	135.2	167.5	159.5	193.5	185.1	160.0	163.6	148.0	152.1
Y	30.8	31.2	19.3	18.9	19.4	18.8	16.9	17.1	17.1	16.8	17.9	17.2	18.6	18.3	18.0	18.5	17.4	17.1	16.7	17.2
La	36.3	35.2	15.4	15.8	17.1	16.8	22.6	21.7	21.3	21.5	20.9	21.2	24.7	24.1	24.1	23.2	24.1	23.8	23.3	23.9
Ce	76.9	75.2	32.0	33.2	36.0	35.2	42.6	43.2	43.6	41.9	41.6	42.3	48.3	47.9	45.6	44.9	45.7	45.2	45.8	44.9
Pr	8.96	8.52	4.35	4.71	4.62	4.44	5.25	5.37	5.24	5.01	5.14	4.93	5.71	5.54	5.36	5.59	5.72	5.45	5.51	4.89
Nd	35.8	36.4	17.7	18.1	18.6	18.4	19.9	20.2	19.2	18.8	20.2	20.4	22.3	22.6	20.6	19.9	21.4	22.3	22.3	22.5
Sm	7.14	7.01	4.12	3.93	3.88	4.07	3.75	3.83	4.11	3.95	3.99	4.05	4.39	4.09	3.71	3.91	3.86	4.01	4.00	3.89
Eu	1.69	1.58	1.22	1.17	1.15	1.11	1.05	0.98	1.15	1.19	1.15	1.13	1.11	1.15	0.91	1.08	1.18	1.21	1.09	1.12
Gd	6.69	6.35	4.12	3.93	4.22	4.17	3.53	3.61	3.73	3.68	3.80	3.75	3.67	3.86	3.33	3.52	3.49	3.62	3.57	3.49
Tb	1.04	1.11	0.61	0.56	0.65	0.61	0.57	0.59	0.58	0.58	0.59	0.60	0.60	0.63	0.51	0.56	0.58	0.57	0.54	0.55
Dy	5.64	5.23	3.44	3.61	3.74	3.54	2.91	3.11	3.36	3.21	3.23	3.39	3.51	3.33	2.97	3.08	3.32	3.45	3.01	2.96
Ho	1.10	1.05	0.74	0.72	0.75	0.73	0.60	0.62	0.73	0.68	0.69	0.72	0.65	0.63	0.65	0.69	0.63	0.66	0.61	0.67

Table 2. *Continuation.*

Sample	GCH-171	GCH-92	GCH-119	GCH-153	GCH-131	GCH-179	GCH-60	GCH-17	GCH-140	GCH-35	GCH-160	GCH-183	GCH-16	GCH-71	GCH-57	GCH-86	GCH-40	GCH-31	GCH-27	GCH-49
Er	3.20	3.11	1.81	1.87	1.99	1.92	1.78	1.81	1.90	1.94	1.92	1.95	1.88	1.83	1.90	1.94	2.06	1.98	1.79	1.85
Tm	0.44	0.41	0.30	0.29	0.30	0.30	0.27	0.28	0.27	0.28	0.29	0.29	0.29	0.29	0.29	0.28	0.28	0.27	0.30	0.30
Yb	2.91	2.76	1.95	1.91	1.92	1.89	1.70	1.72	1.84	1.86	1.73	1.87	1.87	1.92	1.91	1.88	1.84	1.87	1.71	1.73
Lu	0.46	0.48	0.31	0.30	0.31	0.31	0.27	0.28	0.29	0.27	0.28	0.29	0.32	0.30	0.31	0.30	0.31	0.31	0.28	0.29
Nb/Th	3.07	2.757	2.68	2.42	2.80	2.25	2.49	2.54	2.96	2.76	2.86	3.04	2.29	2.35	2.46	2.54	2.36	2.2	2.47	2.49
Ba/Sr	0.63	0.67	0.62	0.63	0.67	0.64	0.85	0.93	0.66	0.66	0.62	0.62	1.09	1.06	2.02	1.73	1.25	1.27	1.43	1.36
Th/Yb	3.13	3.44	1.90	2.25	2.14	2.54	3.59	3.6	2.66	2.74	2.89	2.57	3.85	3.59	4.08	3.94	3.64	3.8	3.63	3.64
La/Nb	1.30	1.34	1.56	1.52	1.49	1.56	1.49	1.37	1.47	1.52	1.46	1.45	1.50	1.49	1.25	1.23	1.53	1.53	1.52	1.52
$(La/Sm)_N$	3.20	3.16	2.35	2.53	2.77	2.60	3.79	3.56	3.26	3.42	3.29	3.29	3.54	3.71	4.09	3.73	3.93	3.73	3.66	3.86
Eu/Eu*	0.75	0.72	0.91	0.91	0.87	0.82	0.88	0.81	0.90	0.95	0.90	0.89	0.85	0.88	0.79	0.89	0.98	0.97	0.88	0.93
$(Gd/Yb)_N$	1.85	1.86	1.70	1.66	1.77	1.78	1.68	1.69	1.64	1.60	1.77	1.62	1.58	1.62	1.41	1.51	1.53	1.56	1.64	1.63

4.09 (average 3.37), which display moderate enrichment of light rare earth elements (LREE). Eu anomaly is calculated by $Eu/Eu*=Eu_N/(Sm_N \times Gd_N)^{1/2}$ (Taylor and McLennan, 1985). Eu anomaly values range from 0.72 to 0.97 (average 0.87), which represent weakly negative Eu anomaly (Ketchum *et al.*, 2013), and Gd_N/Yb_N values range from 1.41 to 1.86 (average 1.65). These ratios reflect nearly flat heavy rare earth element (HREE) on the normalized REE patterns compared to chondrite values (Li *et al.*, 2013).

Zircon U-Pb dating

The outcomes of U-Pb zircon analysis on the two oldest and youngest samples based on the relative age are presented in **Table 3** (No. GCh-119- Hornblende pyroxene olivine basaltic andesite (oldest unit) and No. GCh-171- Pyroxene andesite (youngest unit). Cathodoluminescence (CL) images mostly show oscillatory or growth zoning on zircons (**Fig. 8**), consistent with igneous origin and their growth by magmatic processes (Hoskin and Schaltegger, 2003). The studied zircons have a subhedral to euhedral shape but zircons in the Hornblende pyroxene olivine basaltic andesite rock have a light pink color and in the Pyroxene andesite rock are white to colorless. The Zircons are 100–250 μm in length and 50–100 μm width and have high contents of Th (201–535 ppm) and U (332–1005 ppm) with Th/U varying from 0.572 to 1.45. The results of computing isotopic age of the Hornblende pyroxene olivine basaltic andesite are shown as concordia (**Fig. 9a**). With regard to 15 analyzed points, the average age (Weighted mean) is 5.47 ± 0.22 Ma (errors shown are 1σ). The results of the calculating isotopic age of the Pyroxene andesite are displayed as concordia in **Fig. 9b**. Based on 14 analyzed points, the average age (weighted
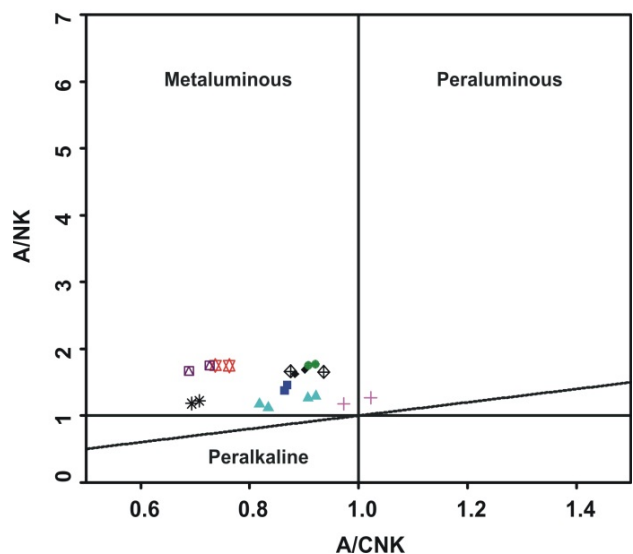

Fig. 5. *A/NK (molar) vs. A/CNK diagram of Shand (1943). The symbols are the same as in Fig. 4.*
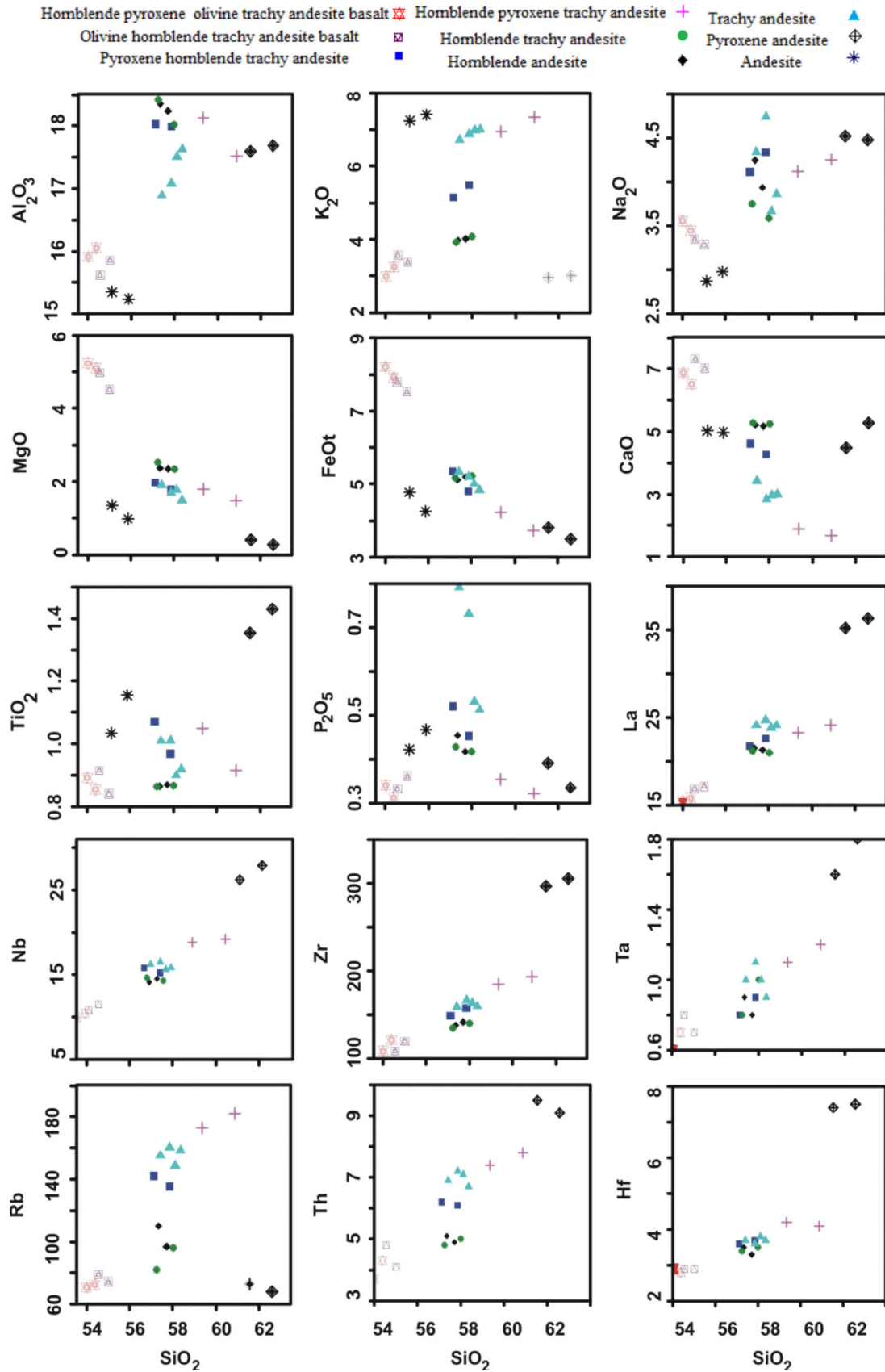
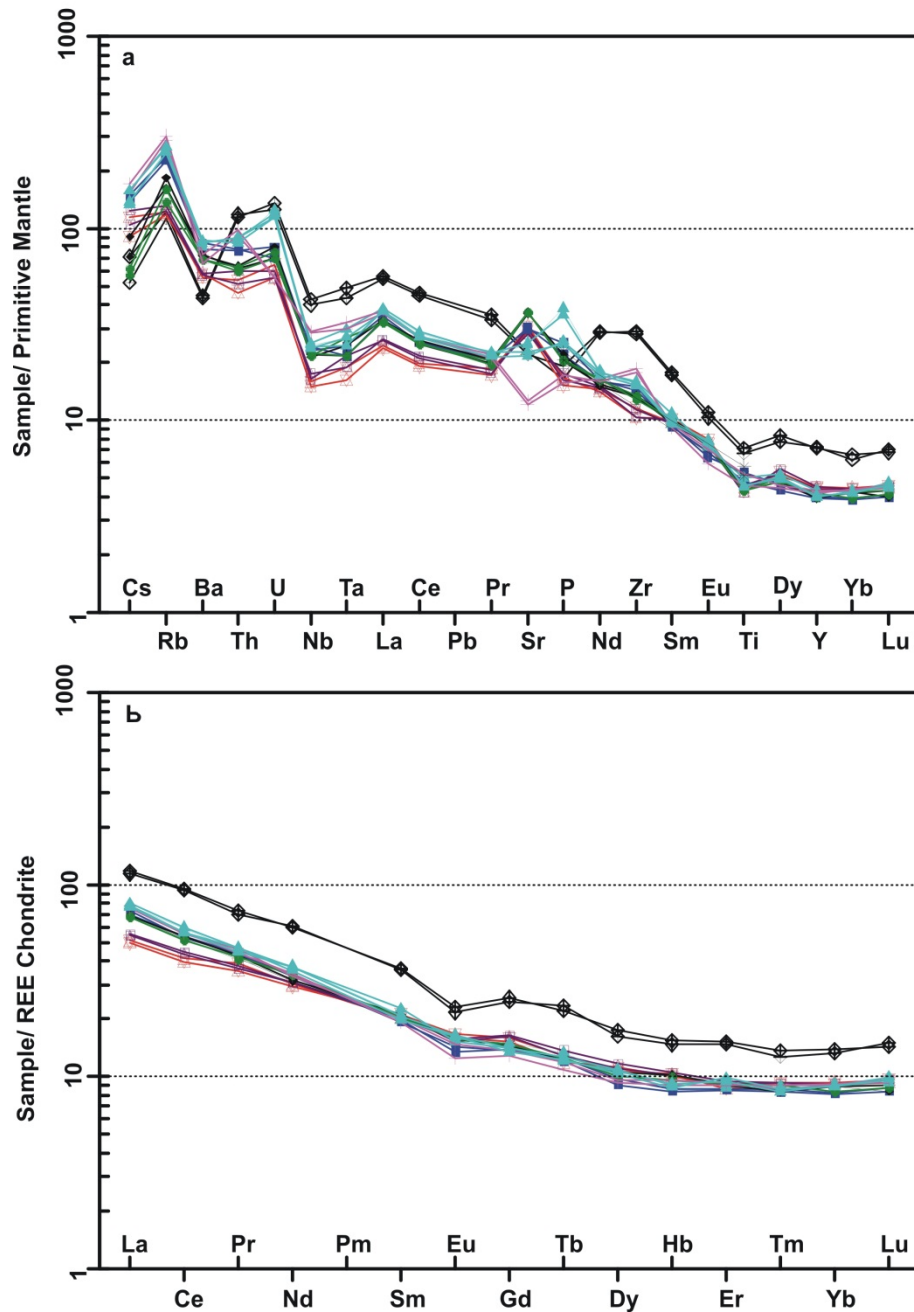**Fig. 6.** *Selected major and trace elements vs. SiO2 contents for the Gandab volcanic rocks.*

Fig. 7. *(a) primitive-mantle normalized diagrams (McDonough and Sun, 1995); (b) REE chondrite normalized diagrams (Boynton, 1984). The symbols are the same as in Fig. 6.*

mean) is 2.44 ± 0.79 Ma (errors shown are 1σ). Therefore, U-Pb zircon age data indicates that Gandab volcanic rocks have been formed in Pliocene time.

Sr-Nd isotopes

Sr and Nd isotopic data obtained in four selected samples are presented in **Table 4**. These samples have ^{143}Nd/^{144}Nd and ^{87}Sr/^{86}Sr ratios ranging from 0.512807 to 0.512893 and from 0.704082 to 0.705931, respectively. If the Nd isotopic ratio composition is expressed using εNd

notation, the range goes from +3.3 to +5.0. Sr and Nd isotopic ratios and εNd values show insignificant differences between present-day values and calculated initial values for young geological ages, like those obtained in this work (less than 6 Ma), since both ^{87}Rb and ^{147}Sm have very low decay constants (Steiger and Jager, 1977; Villa *et al.*, 2015). Therefore, the measured isotopic ratios, in this case may be considered as the representing initial compositions.

Table 3. *Zircon U–Pb isotopic data for the Gandab volcanic rocks.*

Sample No.	U^{238} (ppm)	Th^{232}/U^{238}	$^{207}Pb/^{206}Pb$	$^{238}U/^{206}Pb$	$^{206}Pb/^{238}U$	Age (Ma)	± (Ma)
GCh-119-1	343	0.730	0.0424	1234.01	0.0008	5.2	0.1
GCh-119-2	363	0.889	0.0514	1185.23	0.0008	5.4	0.2
GCh-119-3	347	0.579	0.0622	1197.66	0.0008	5.3	0.2
GCh-119-4	348	0.621	0.1039	1247.21	0.0008	4.9	0.1
GCh-119-5	389	1.113	0.0750	1173.23	0.0008	5.3	0.2
GCh-119-6	401	1.314	0.0922	1125.15	0.0009	5.5	0.1
GCh-119-7	456	0.967	0.0561	1192.12	0.0008	5.3	0.1
GCh-119-8	372	0.871	0.0748	1134.21	0.0009	5.5	0.2
GCh-119-9	339	0.690	0.0621	1179.10	0.0008	5.3	0.2
GCh-119-10	375	0.821	0.0940	1211.12	0.0008	5.1	0.1
GCh-119-11	332	1.101	0.1175	1045.23	0.0009	5.8	0.2
GCh-119-12	431	0.821	0.0920	1119.12	0.0009	5.6	0.2
GCh-119-13	369	1.451	0.0831	1131.57	0.0009	5.5	0.2
GCh-119-14	367	0.781	0.1751	980.56	0.0010	6.1	0.1
GCh-119-15	383	0.983	0.1669	960.13	0.0010	6.3	0.2
GChH-171-1	973	0.865	0.0798	2886.14	0.0003	2.1	0.1
GCh-171-2	613	0.550	0.0533	2819.62	0.0004	2.3	0.1
GCh-171-3	797	0.943	0.0904	2690.01	0.0004	2.4	0.1
GCh-171-4	765	0.595	0.0983	2911.14	0.0003	2.1	0.1
GCh-171-5	821	1.123	0.1289	2248.87	0.0004	2.7	0.1
GCh-171-6	678	0.871	0.1634	2321.22	0.0004	2.5	0.1
GCh-171-7	587	0.781	0.0879	2430.76	0.0004	2.5	0.1
GCh-171-8	801	1.121	0.0973	2869.36	0.0003	2.1	0.1
GCh-171-9	745	0.891	0.0611	2856.00	0.0004	2.2	0.1
GCh-171-10	956	1.153	0.1298	2678.87	0.0004	2.4	0.1
GCh-171-11	1005	1.151	0.0518	2488.76	0.0004	2.7	0.1
GCh-171-12	567	0.701	0.0741	2780.20	0.0003	2.3	0.1
GCh-171-13	710	1.151	0.0588	2130.45	0.0005	3.1	0.2
GCh-171-14	834	0.871	0.0741	2414.67	0.0004	2.7	0.1

Table 4. *Rb–Sr and Sm–Nd isotopic data of the Gandab volcanic rocks (Entezari et al., 2016). 2σ shows the precision of measurement and calculations (standard error).*

Sample	Latitude (N)	Longitude (E)	Rb (ppm)	Sr (ppm)	$^{87}Rb/^{86}Sr$	$^{87}Sr/^{86}Sr$	Uncertainty (2σ)	Sm (ppm)	Nd (ppm)	$^{147}Sm/^{144}Nd$	$^{143}Nd/^{144}Nd$	Uncertainty (2σ)	εNd
GCh-16	35°49'49"	58°43'14"	106	505	0.609	0.705047	0.000020	4.39	22.3	0.119	0.512833	0.000017	+3.8
GCh-57	35°50'18"	58°42'44"	182	239	2.205	0.705931	0.000020	3.71	20.6	0.109	0.512807	0.000015	+3.3
GCh-171	35°48'59"	58°44'25"	68.0	454	0.433	0.704082	0.000021	7.14	35.8	0.121	0.512893	0.000015	+5.0
GCh-119	35°47'37"	58°43'39"	70.8	615	0.333	0.704614	0.000016	4.12	17.7	0.141	0.512843	0.000017	+4.0

Tectonic setting

Application of TiO_2 *vs.* Al_2O_3 (Muller *et al.*, 1992) indicate that all of the samples are located at the arc environment (**Fig. 10a**). Plotting samples on the Nb*50-Zr*/3-Ce/P_2O_5 ternary diagram (Muller *et al.*, 1992) shows that Gandab volcanic rocks are situated at post-collisional arc (**Fig. 10b**).
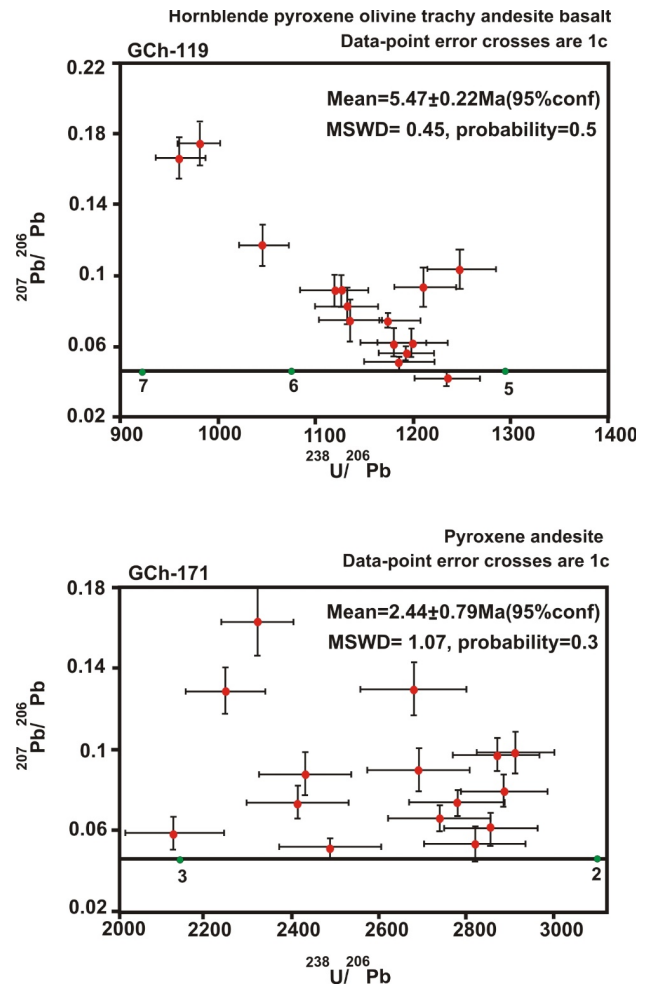
Researchers (e.g. Fang and Niu, 2003) have used Nb/Th ratio to survey the impact of subduction zone processes on the formation of volcanic rocks. This ratio is lower than '4' in the rocks related to the subduction zone (Sun and Mcdonough, 1989). Nb/Th ratio of the proposed samples varies from 2.19 to 3.06. As a result, Nb/Th ratio in the proposed samples is less than '4' and it verifies that

the studied rocks were affected by the processes related to the subduction zone. As it was mentioned earlier, the study area is located at Sabzevar zone (NE Iran). During the Late Cretaceous, the Sabzevar oceanic basin (branch of the Neo-Tethys Ocean between central Iranian microcontinent and Eurasian margin) was formed, which was later closed during Palaeocene-Eocene (Rossetti *et al.*, 2010). With regard to the ages (5.47 to 2.44 Ma) and geochemical properties of the Gandab volcanic rocks, we believe that they have been created in post-collision environment after Neo-Tethys subduction. Enrichment in LILE and LREE relative to HFSE and HREE respectively, and negative anomalies of Nb–Ti elements are the specifications of subduction-related magmas. These characteristics are generally related to a mantle source, which
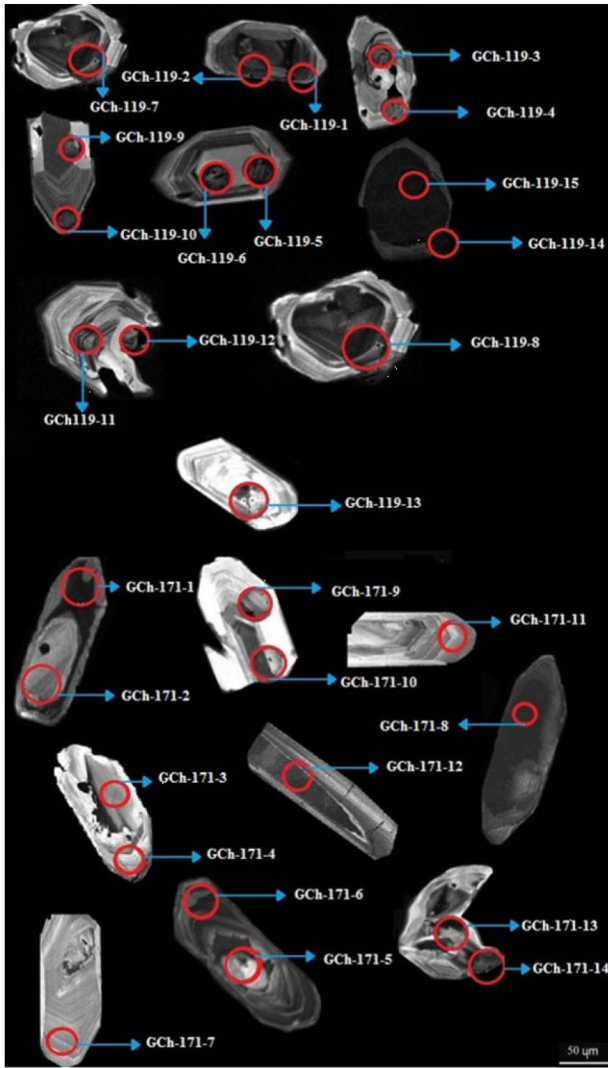
Fig. 8. *Cathodoluminescence images of analysed zircon grains from GCh-119 and GCh-171 samples, for the investigated volcanic rocks from the Gandab area, Iran. The red circles show the analyzed spots.*

Fig. 9. *Concordia diagrams of $^{207}Pb/^{207}Pb$ vs. $^{238}U/^{206}Pb$ for calculating the age of zircons from Gandab volcanic rocks (Age is reported in Ma, GCh-119 = 5.47 ± 0.22, GCh-171 = 2.44 ± 0.79).*

has already been enriched in LILE and LREE over HFSE and HREE by metasomatic activity of solutions released from the subducted sediments or slab (Pearce, 1983; Cameron *et al.*, 2003). Many different types of models have been suggested to illustrate this signature in the post-collisional setting such as considering amphibolites, peridotite, and metapelite as a hybrid source in the crust–mantle boundary (López-Moro and López-Plaza, 2004), or presenting a theory regarding mixing of magmas in the asthenosphere and enriched lithospheric mantle (Li *et al.*, 2000). Considering all evidences, the best suggestion can be an enrichment of lithospheric mantle by earlier subduction events in a post-collision stage (Turner *et al.*, 1996; Janous'ek *et al.*, 2000; Liu *et al.*, 2002; Aydin *et al.*, 2008).

Petrogenetic properties

Calculated ages based on U-Pb zircon and geochemical characteristics indicate that all volcanic rocks of the Gandab area probably have a similar petrogenesis and magma source. Changing major and trace elements normally display linear trends *vs.* SiO$_2$ (**Fig. 6a-6o**) indicating that the volcanic rocks were resulted from same parent magma. The inverse correlation can be seen between SiO$_2$ and CaO, FeO and MgO in the volcanic rocks. As well, SiO$_2$ has a direct coloration with Na$_2$O, K$_2$O, Al$_2$O$_3$, La, Nb, Zr, Rb, Th, Ta and Hf. As a result, crystal fractionation proccess is specified from the parental magma.
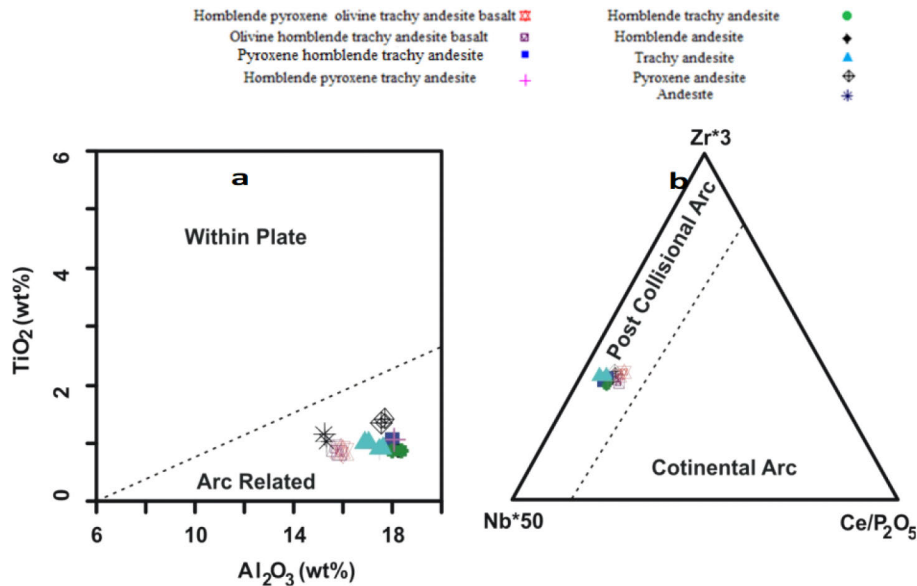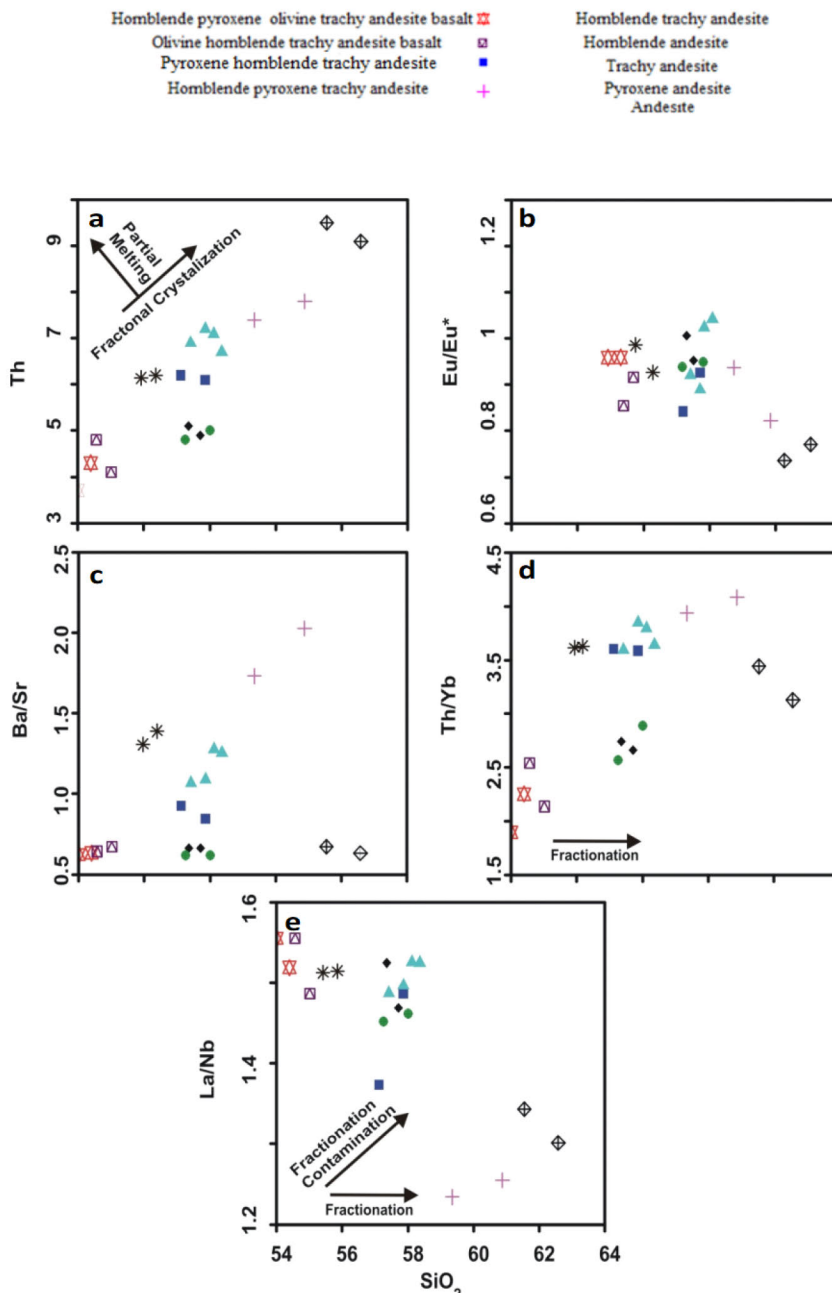
Fig. 10. *(a) TiO₂ vs. Al₂O₃ diagram, (Muller et al., 1992); (b) Nb*50-Zr*/3-Ce/P2O5 ternary diagram (Muller et al., 1992).*

Furthermore, **Fig. 9** depicts REE chondrite-normalized diagrams, and it is clear that HREE includes the limited variations, while LREE comprises higher variations. The above mentioned patterns demonstrate a crystal fractionation or a partial melting process including mineral phases that powerfully fractionate or partial melting LREE relative to HREE (Lopez-Moro and Lopez-Plaza, 2004; Lopez-Moro *et al.*, 2012). It should be remarked that it s very difficult to distinguish the difference between fractional crystallization and partial melting based on the primary magma compositions. But, this difference can be distinguished based on the incompatible element plots such as the plot of Th versus SiO_2 shown in **Fig. 11**, that is a representing fractional crystallization process (Whalen *et al.*, 1987). The relationship between Eu/Eu* and SiO_2 (Irber, 1999) in the Gandab volcanic rocks is depicted in **Fig. 11b** and this inverse correlation between Eu/Eu* and SiO_2 indicates a fractionation sequence in the rocks of area. **Fig. 11c** also shows a direct correlation between Ba/Sr ratio and SiO_2 (Lopez-Moro *et al.*, 2012), which indicates the process of crystal fractionation in volcanic rocks surrounding Gandab. In the mantle-derived rocks, the ratio of Th/Yb and La/Nb is sensitive to the crustal contamination (Taylor and McLennan, 1985). The ratios of Th/Yb and La/Nb *vs.* SiO_2 in the Gandab samples are depicted in **Fig. 11d**, **11e** and it is clear that Th/Yb and La/Nb ratios show a little variation to the SiO_2. This issue is an indication of crystal fractionation. Furthermore, lack of mafic microgranular enclaves and disequilibrium textures such as sieve texture and antirapakivi indicate that magma mixing has not occurred in the volcanic rocks of area.

Source properties

Negative and positive εNd (t) isotopic ratios demonstrate the features of the crustal melt, and mantle array, respectively (Kemp *et al.*, 2007; Yang *et al.*, 2007; Li *et al.*, 2009). With respect to the $\varepsilon Nd_i – (^{87}Sr/^{86}Sr)_i$ isotopic plot depicted in **Fig. 12**, the Gandab Volcanic rocks show a trend toward the mantle (Kemp *et al.*, 2007; Li *et al.*, 2009).

The Gandab samples are mainly characterized with high concentrations of incompatible trace elements (e.g., LILE and LREE). Moreover, **Fig. 7** shows that these samples are marked by considerable negative Nb, Ta, and Ti anomalies specifying that the samples have not been driven from normal MORB or OIB mantle sources which usually demonstrate positive Nb–Ti anomalies in primitive-mantle normalized trace element diagrams (Hofmann, 1997). As well, the Nb/La ratios of the Gandab samples are changed from 0.64 to 0.79 representing a lithospheric mantle source (Bradshaw and Smith, 1994; Smith *et al.*, 1999). Hydrous phase formed in the lithospheric mantle source can be shown based on the difference between element compatibility of phlogopite and amphibole (Furman and Graham, 1999; Yang *et al.*, 2004). Since the Rb/Sr ratios of volcanic rocks reflect the Rb/Sr ratios of their source rocks (Kemp and Hawkesworth, 2003), the Gandab volcanic rocks have high Rb/Sr ratios, but a low initial $^{87}Sr/^{86}Sr$ ratio is also seen which probably shows a mica-bearing source with a short residence time within the mantle. In the study area, the Ba/Rb (2.51–5.51) and Nb/Th (2.19–3.06) ratios are relatively low (**Table 2**), while the Rb/Sr ratios (0.11–0.76) are relatively high. As a result, the source region includes phlogopite instead of amphibole. Spinel is de-

Hornblende pyroxene olivine trachy andesite basalt ⬡
Olivine hornblende trachy andesite basalt ⬡
Pyroxene hornblende trachy andesite ■
Hornblende pyroxene trachy andesite +

Hornblende trachy andesite
Hornblende andesite
Trachy andesite
Pyroxene andesite
Andesite

Fig. 11. *Diagrams showing fractional crystalliza-tion (FC) for Gandab volcanic rocks. (a) Th vs. SiO_2 (Whalen et al., 1987); (b) Eu/Eu* vs. SiO_2 (Irber, 1999); (c) Ba/Sr vs. SiO_2 (Lopez-Moro et al., 2012); (d) Th/Yb vs. SiO_2 (Taylor and McLen-nan, 1985); (e) La/Nb vs. SiO_2 (Taylor and McLennan, 1985).*

pleted from HREE and Y, while garnet and amphibole are enriched in HREE, Y, and Middle REE (MREE), respectively. Values of La_N / Yb_N ratio in the Gandab samples are changed from 5.32 to 9.31. As well, this ratio is less than the La_N / Yb_N ratio in the igneous rocks in which have been derived from the magma with garnet as the major phase in their source (Martin, 1987), represent-ing the garnet as the major residual phase. Therefore, spinel and/or amphibole may be existent in the residua. Nevertheless, the trivial enrichment in MREE of the samples (**Fig. 7**) indicates that amphibole may not stay stable in the residual following fractional melting. Geo-chemical and isotopic characteristics of the samples in the

study area demonstrate that the phlogopite-bearing spinel peridotite is the source of magma which formed the vol-canic rocks of the area.

6. CONCLUSIONS

LA–ICP–MS U-Pb zircon age data indicate that the volcanic rocks have been formed between 5.47 ± 0.22 Ma and 2.44 ± 0.79 Ma. Major oxides geochemistry reveal that all the studied rocks are typically metaluminous. In primitive mantle and chondrite-normalized trace element spider diagrams, the analyzed samples demonstrate slight to moderate enrichment in LILE ($2.35 \leq La_N / Sm_N \leq 4.09$)
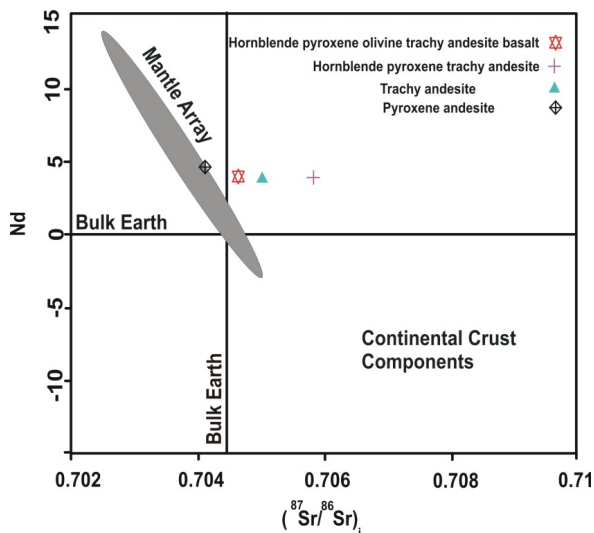
Fig. 12. *Plot of initial ($^{87}Sr/^{86}Sr$)$_i$ vs. εNd ratios (Entezari et al., 2016).*

compared to HFSE ($1.41 \leq Gd_N/Yb_N \leq 1.86$) while being accompanied by negative anomalies of Nb and Ti. These geochemical properties and isotope geochemistry (Sr$_i$ and εNd_i) illustrate that the studied rocks are derived from enriched lithospheric mantle source as well as they are co-genetic which fractional crystallization process has produced different magmas in their composition. The analyzed samples also show a post-collisional arc environment. We propose that volcanic activity in Gandab area during Pliocene period has been created by the enriched lithospheric mantle source which is metasomatized by previously subducted sediments after Neo-Tethys subduction.

ACKNOWLEDGMENT

REFERENCES

Alavi M, 1991. *Tectonic map of the Middle East, scale 1:2,900,000.* Geological Survey of Iran.

Aydin F, Karsli O and Chen B, 2008. Petrogenesis of the Neogene alkaline volcanic with implications for post collisional lithospheric thinning of the Eastern Pontides, NE Turkey. *Lithos* 104: 249–266, DOI 10.1016/j.lithos.2007.12.010.

Baker J, Peate D, Waight T and Meyzen C, 2004. Pb isotopic analysis of standards and samples using a Pb-207-Pb-204 double spike and thallium to correct for mass bias with a double-focusing MC-ICP-MS. *Chemical Geology* 211: 275–303, DOI 10.1016/j.chemgeo.2004.06.030.

Berberian M and King GCP, 1981. Towards a paleogeography and tectonic evolution of Iran. *Canadian Journal of Earth Sciences* 18: 210–265, DOI 10.1139/e81-019.

Black LP and Gulson BL, 1978. The age of the Mud tank Carbonatite, Strangways Range, Northern Territory. *BMR Journal of Australian Geology and Geophysics* 3: 227–232.

Black LP, Kamos L, Allen CM, Aleinikoff JN, Davis DW, Korsch RJ and Foudoulis C, 2003. TEMORA 1: a new zircon standard for Phanerozoic U-Pb geochronology. *Chemical Geology* 200: 155–170, DOI 10.1016/S0009-2541(03)00165-7.

Black LP, Kamo SL, Allen CM, Davis DW, Aleninikoff JN, Valley JW, Mundil R, Campbell IH, Korsch RJ, Williams IS and Foudoulis C, 2004. Improved $^{206}Pb/^{238}U$ microprobe geochronology by the monitoring of a trace-element related matrix effect; SHRIMP, ID-TIMS, ELA-ICP-MS, and oxygen isotope documentation for a series of zircon standards. *Chemical Geology* 205: 115–140, DOI 10.1016/j.chemgeo.2004.01.003.

Boynton WVZ, 1984. *Geochemistry of the rare earth elements: meteorite studies.* Rare Earth Element Geochemistry (Henderson, P., ed.). Elsevier, Amsterdam, 63–114.

Bradshaw TK and Smith EI, 1994. Polygenetic Quaternary volcanism at Crater Flat, Nevada. *Journal of Volcanology and Geothermal Research* 63: 165–182, DOI 10.1016/0377-0273(94)90072-8.

Cameron BI, Walker JA, Carr MJ, Patino LC, Matias O, Feigenson MD, 2003. Flux versus decompression melting at stratovolcanoes in southeastern Guatemala. *Journal of Volcanology and Geothermal Research* 119: 21–50, DOI 10.1016/S0377-0273(02)00304-9.

Entezari Harsini A, Mazaheri SA, Saadat S and Santos JF, 2016. Geochemistry, petrology, and mineralization in volcanic rocks located in south Neyshabour, NE Iran. *Journal of Mining and Environment* 8: 139–154, DOI 10.22044/jme.2016.766.

Esmaiely D, Nédéléc A, Valizadeh MV, Moore F and Cotton J, 2005. Petrology of the Jurassic Shah-Kuh granite (eastern Iran), with reference to tin mineralization. *Journal of Asian Earth Sciences* 25: 961–980, DOI 10.1016/j.jseaes.2004.09.003.

Fang N and Niu Y, 2003. Late Palaeozoic ultramafic lavas in Yunnan, SW China, and their geodynamic significance. *Journal of Petrology* 44: 141–158. DOI 10.1093/petrology/44.1.141.

Furman T and Graham D, 1999. Erosion of lithospheric mantle beneath the East African Rift system: geochemical evidence from the Kivu volcanic province. *Lithos* 48: 237–262, DOI 10.1016/S0024-4937(99)00031-6.

Ghalamghash J, Bouchez JL, Vosoughi-Abedini M and Nédélec A, 2009. The Urumieh Plutonic Complex (NW Iran): Record of the geodynamic evolution of the Sanandaj – Sirjan zone during Cretaceous times – Part II: Magnetic fabrics and plate tectonic reconstruction. *Journal of Asian Earth Sciences* 36: 303–317, DOI 10.1016/j.jseaes.2009.06.002.

Halpin JA, Jensen T, McGoldrick P, Meffre S, Berry RF, Everard JL, Calver CR, Thompson J, Goemann K and Whittaker JM, 2014. Authigenic monazite and detrital zircon dating of the Proterozoic Rocky Cape Group, Tasmania: Links to the Belt-Purcell Supergroup, North America. *Precambrian Research* 250: 50–67, DOI 10.1016/j.precamres.2014.05.025.

Hatzfeld D and Molnar P, 2010. Comparisons of the kinematics and deep structures of the Zagros and Himalaya and of the Iranian and Tibetan Plateaus, and geodynamic implications. *Reviews of Geophysics* 48: RG2005, DOI 10.1029/2009RG000304.

Hofmann AW, 1997. Mantle geochemistry: the message from oceanic volcanism. Nature 385: 219–229, DOI 10.1038/385219a0.

Hoskin PWO and Schaltegger U, 2003. The composition of zircon and igneous and metamorphic petrogenesis. In: Manchar, J.M., Hoskin, P.W.O. (Eds.), *Zircon: Reviews of Mineralogy and Geochemistry* 53: 27–62, DOI 10.2113/0530027.

Irber W, 1999. The lanthanide tetrad effect and its correlation with K/Rb, Eu/Eu*, Sr/Eu, Y/Ho, and Zr/Hf of evolving peraluminous granite suites. *Geochimica at Cosmochimica Acta* 63: 489–508, DOI 10.1016/S0016-7037(99)00027-7.

Irvine TN and Baragar WRA, 1971. A guide to the chemical classification of the common volcanic rocks. *Canadian Journal of Earth Sciences* 8: 523–548, DOI 10.1139/e71-055.

Jackson SE, Pearson NJ, Griffin WL and Belousova EA, 2004. The application of laser ablation-inductively coupled plasma-mass spectrometry to in situ U-Pb zircon geochronology. *Chemical Geology* 211: 47–69, DOI 10.1016/j.chemgeo.2004.06.017.

Janous'ek V, Bowes DR, Rogers G, Farrow CM and Jelinak E, 2000. Modelling diverse processes in the petrogenesis of a composite batholith: the Central European Hercynides. *Journal of Petrology* 41: 511–543, DOI 10.1093/petrology/41.4.511.

Kemp AIS and Hawkesworth CJ, 2003. Granitic perspectives on the generation and secular evolution of the continental crust. In: Rudnick, R.L. (Ed.), the Crust. Treatise on Geochemistry, 3. Elsevier, Pergamon, pp. 349–410.

Kemp AIS, Hawkesworth CJ, Foster GL, Paterson BA, Woodhead JD, Hergt JM, Gray CM and Whitehouse MJ, 2007. Magmatic and crustal differentiation history of granitic rocks from Hf-O isotopes in zircon. *Science* 315: 980–983, DOI 10.1126/science.1136154.

Ketchum KY, Heaman LM, Bennett G and Hughesa DJ, 2013. Age, petrogenesis and tectonic setting of the Thessalon volcanic rocks, Huronian Supergroup, Canada. *Precambrian Research* 233: 144–172, DOI 10.1016/j.precamres.2013.04.009.

Kosler J, 2001. Laser-ablation ICPMS study of metamorphic minerals and processes. In: Sylvester P. J. ed. Laser-ablation-ICPMS in the earth sciences; principles and applications. *Mineralogical Association of Canada Short Course Handbook* 29: 185–202.

Li X, Long WG, Li QL, Liu Y, Zheng YF, Yang YH, Chamberlain KR, Wan DF, Guo CH, Wang XC and Tao H, 2010. Penglai Zircon Megacrysts: A Potential New Working Reference Material for Microbeam Determination of Hf-O Isotopes and U-Pb Age. *Geostandards and Geoanalytical Research* 34: 117–134.

Li XH, Li WX, Wang XC, Li QL, Liu Y and Tang GQ, 2009. Role of mantle-derived magma in genesis of early Yanshanian granites in the Nanling Range, South China:in situ zircon Hf-O isotopic constraints. *Science in China, Series* 52: 1262–1278.

Li XH, Zhou HW, Liu Y, Le CY, Sun M and Chen ZH, 2000. Shoshonitic intrusive suite in SE Guangxi: petrology and geochemistry. *Chinese Sciences Bulletin* 45: 653–659, DOI 10.1007/BF02886045.

Li XW, Mo XX, Yu XH, Ding Y, Huang XF, Wei P and He WY, 2013. Petrology and geochemistry of the early Mesozoic pyroxene andesites in the Maixiu Area, West Qinling, China: Products of subduction or syn-collision? *Lithos* 172–173: 158–174, DOI 10.1016/j.lithos.2013.04.010.

Liu H, Qiu JS, Luo QH, Xu XS, Ling WL and Wang DZ, 2002. Petrogenesis of the Mesozoic potash-rich volcanic rocks in the Luzong basin, Anhui Province: geochemical constrains. *Geochemica* 31: 129–140.

López-Moro FJ, López Plaza M and Romer RL, 2012. Generation and emplacement of shear-related highly mobile crustal melts: the syn-kinematic leucogranites from the Variscan Tormes Dome, Western Spain. *International Journal of Earth Sciences* 101: 1273–1298, DOI 10.1007/s00531-011-0728-1.

López-Moro FJ and López-Plaza M, 2004. Monzonitic series from the Variscan Tormes Dome (Central Iberian Zone): petrogenetic evolution from monzogabbro to granite magmas. *Lithos* 72: 19–44, DOI 10.1016/j.lithos.2003.08.002.

Martin H, 1987. Petrogenesis of Archean trondhjemites, tonalites and granodiorites from eastern Finland: major and trace element geochemistry. *Journal of Petrology* 28: 921–953.

Mazhari SA, Amini S, Ghalamghash J and Bea F, 2011. Petrogenesis of granitic unit of Naqadeh complex, Sanandaj-Sirjan Zone, NW Iran. *Arabian Journal of Geosciences* 4: 59–67, DOI 10.1007/s12517-009-0077-6.

McDonough WF and Sun SS, 1995. The composition of the Earth. Chemical Geology 120: 223–253, DOI 10.1016/0009-2541(94)00140-4.

Middlemost EAK, 1994. Naming materials in the magma/igneous rock system. *Earth-Science Reviews* 37: 215–244, DOI 10.1016/0012-8252(94)90029-9.

Muller D, Rock NMS and Groves DI, 1992. Geochemical discrimination between shoshonitic and potassic volcanic rocks in different tectonic setting: a pilot study. *Mineralogy and Petrology* 46: 259–286, DOI 10.1007/BF01173568.

Naderi Mighan N, 2000. *Geological map of Kadkan, scale 1:100,000*. Geological Survey of Iran.

Paton C, Woodhead JD, Hellstrom JC, Hergt JM, Greig A and Maas R, 2010. Improved laser ablation U-Pb zircon geochronology through robust downhole fractionation correction. *Geochemistry, Geophysics, Geosystems* 11: 1525–2027, DOI 10.1029/2009GC002618.

Pazirandeh M, 1973. Distribution of volcanic rocks in Iran and a preliminary discussion of their relationship to tectonics. *Bulletin Volcanologique* 37: 573–585.

Pearce JA, 1983. Role of the sub-continental lithosphere in magma genesis at active continental margins. In: Hawkesworth, C.J., Norry, M.J. (Eds.), Continental Basalts and Mantle Xenoliths. Shiva, Nantwich, Cheshire, UK, pp. 230–250.

Rossetti F, Nasrabady M, Vignaroli G, Theye T, Gerdes A, Razavi MH and Vaziri HM, 2010. Early Cretaceous migmatitic mafic granulites from the Sabzevar range (NE Iran): implications for the closure of the Mesozoic peri-Tethyan oceans in central Iran. *Terra Nova* 22: 26–34, DOI 10.1111/j.1365-3121.2009.00912.x.

Ruttner A and Stöcklin J, 1967. Geological map of Iran, scale 1:100,000, Geological Survey of Iran. *Science Reviews* 37: 215–224.

Saadat S and Stern ChR, 2016. Distribution and geochemical variations among paleogene volcanic rocks from the north-central Lut block, eastern Iran. *Iranian Journal of Earth Sciences* 8: 1–24.

Saadat S, Karimpour MH and Stern ChR, 2010. Petrochemical characteristics of Neogene and Quaternary alkali olivine basalts from the western margin of the Lut block, eastern Iran. *Iranian Journal of Earth Sciences* 2: 87–106.

Sengor AMC, 1990. A new model for the Late Paleozoic-Mesozoic tectonic evolution of Iran and implications for Oman. In: Robertson, A.H.F., Searle, M.P., Ries, A.C., (eds.). The Geology and Tectonics of the Oman Region. *Geological Society of London Special Publication* 49: 797–831.

Shafaii Moghadam HS, Corfu F, Chiaradia M, Stern RJ and Ghorbani G, 2014. Sabzevar Ophiolite, NE Iran: Progress from embryonic oceanic lithosphere into magmatic arc constrained by new isotopic and geochemical data. Lithos 210–211: 224–241, DOI 10.1016/j.lithos.2014.10.004.

Shand SJ, 1943. *The eruptive rocks: 2nd edition*, John Wiley, New York, 444p.

Slama J, Kosler J, Condon DJ, Crowley JL, Gerdes A, Hanchar JM, Horstwood MSA, Morris GA, Nasdala L, Norberg N, Schaltegger U, Schoene B, Tubrett MN and Whitehouse MJ, 2008. Plesovice zircon - A new natural reference material for U-Pb and Hf isotopic microanalysis. Chemical Geology 249: 1–35, DOI 10.1016/j.chemgeo.2007.11.005.

Smith EI, Sánchez A, Walker JD and Wang K, 1999. Geochemistry of mafic magmas in the Hurricane volcanic field, Utah: implications for small- and large-scale chemical variability of the lithospheric mantle. *Journal of Geology* 107: 433–448, DOI 10.1086/314355.

Spies O, Lensch G, Mihem A, 1983. Geochemistry of the postophiolitic Tertiary volcanics between Sabzevar and Quchan (NE Iran). *Rep. Geological Survey of Iran* 51: 247–266.

Steiger RH and Jäger E, 1977. Subcommision on geochronology: convention in the use of decay-constants in geo- and cosmochemistry. *Earth and Planetary Science Letters* 36: 359–362, DOI 10.1016/0012-821X(77)90060-7.

Sun SS and McDonough WF, 1989. *Chemical and isotopic systematics of oceanic basalts: implications for mantle composition and processes*. IIn: Saunders, A.D., Norry, M.J. (Editors). Magmatism in the Ocean Basins, Geological Society, London, Special Publications 42: 313–345.

Tarkian M, Bock WD and Neumann M, 1983. Geology and mineralogy of the Cu−Ni−Co−U ore deposits at Talmessi and Meeskani, central Iran. *Tschermaks mineralogische und petrographische Mitteilungen* 32: 111–133, DOI 10.1007/BF01081105.

Taylor SR and McLennan SM, 1985. *The continental crust: Its composition and evolution*. Oxford, 311pp.

Turner S, Arnaud N, Liu J, Rogers N, Hawkesworth C, Harris N, Kelley S, Van Calsteren P, Deng W, 1996. Post-collision shoshonitic volcanism on the Tibetan Plateau: implications for convective thinning of the lithosphere and the source of ocean island basalts. *Journal of Petrology* 37: 45–71, DOI 10.1093/petrology/37.1.45.

Villa IM, De Bièvre P, Holden NE, Renne PR, 2015. IUPAC-IUGS recommendation on the half life of [87]Rb. *Geochimica et Cosmochimica Acta* 164: 382–385, DOI 10.1016/j.gca.2015.05.025.

Whalen JB, Currie KL and Chappell BW, 1987. A-type granites: Geochemical characteristics, discrimination and petrogenesis. *Contributions to Mineralogy and Petrology* 95: 407–419, DOI 10.1007/BF00402202.

Wiedenbeck M, Alle P, Corfu F, Griffin WL, Meier M, Oberli F,

Vonquadt A, Roddick JC, Speigel W, 1995. 3 Natural Zircon Standards for U-Th-Pb, Lu-Hf, Trace-Element and REE Analyses. *Geostandards Newsletter* 19: 1–23, DOI 10.1111/j.1751-908X.1995.tb00147.x.

Yang JH, Chung SI, Zhai MG and Zhou XH, 2004. Geochemical and Sr-Nd-Pb isotopic compositions of mafic dykes from the Jiaodong peninsula, China: evidence for veinplus- peridotite melting in the lithospheric mantle. *Lithos* 73: 145–160, DOI 10.1016/j.lithos.2003.12.003.

Yang JH, Wu FY, Wilde SA, Xie LW, Yang YH and Liu XM, 2007. Tracing magma mixing in granite genesis, in situ U-Pb dating and Hf-isotope analysis of zircons. *Contributions to Mineralogy and Petrology* 153: 177–190, DOI 10.1007/s00410-006-0139-7.